Acta Crystallographica Section A
Foundations of Crystallography
ISSN 0108-7673

Received 13 November 2007
Accepted 11 March 2008

Dedicated to Professor George M. Sheldrick on the occasion of his 65th birthday

Foundations of residual-density analysis

Kathrin Meindl and Julian Henn*

Georg-August Universität Göttingen, Tammannstrasse 4, 37077 Göttingen, Germany. Correspondence e-mail: jhenn@chemie.uni-goettingen.de

New and concise descriptors of the residual density are presented, namely the gross residual electrons, the net residual electrons and the fractal dimension distribution. These descriptors indicate how much residual density is present and in what way it is distributed, *i.e.* the extent to which the distribution is featureless. The amount of residual density present accounts for noise in the experimental data as well as for modeling inadequacies. Therefore, the minimization of the gross residual electrons during refinement serves as a quality criterion. In the case where only Gaussian noise is present in the residual density, the fractal distribution is parabolic in shape. Deviations from this shape therefore serve as an indicator for systematic errors. The new measures have been applied to simulated and experimental data in order to study the effects of noise, model inadequacies and truncation in the experimental resolution. These measures, although designed and examined with particular regard to applications of space residual density, are very general and can in principle also be applied to space and momentum residual densities in a one-, two-, three- or higher-dimensional Euclidean space.

1. Abbreviations

General	
$\mathbf{F} = F\exp(i\phi)$	phased structure factor with non-negative amplitude $F = \lvert\mathbf{F}\rvert$ and phase ϕ
$\{\mathbf{F}\}$	a set of structure factors
$\Delta\rho$	difference density obtained from differences in phases and moduli of two sets $\{\mathbf{F_a}\}$, $\{\mathbf{F_b}\}$
ρ_0	residual density: difference density with phases from one set assigned to both sets
Multipole model formalism	
$\rho_{\rm at}$, $\rho_{\rm core}$, $\rho_{\rm valence}$	pseudo-atom density, spherical core and spherical valence density
P_c, P_v, P_{lm}	population parameters
κ, κ'	radial screening parameters for monopoles and multipoles
R_l	radial functions
d_{lm}	real-valued normalized spherical harmonics
P_l^m	associated Legendre functions
Maximum-entropy methods	
S	entropy
ρ_k	density at kth grid point
$\{\rho_k\}$	set of density values
τ_k	reference density, prior density
Residual-density analysis	
$\rho_{\rm net}$	net residual density (e Å^{-3})
$e_{\rm net}$	net residual electrons (e)
$\rho_{\rm gross}$	gross residual density (e Å^{-3})
$e_{\rm gross}$	gross residual electrons (e)
V, $V_{\rm UC}$	volume, volume of the unit cell (Å^3)
$0 \le d^f(\rho_0) \le 3$	dimensionless fractal dimension distribution
$d^f(0)$	fractal dimension at $\rho_0 = 0$
$\Delta\rho_0 = \rho_{0,\max} - \rho_{0,\min}$	span of residual density, flatness (e Å^{-3})

2. Introduction

For two given density distributions ρ_a and ρ_b in a unit cell, the difference distribution $\Delta\rho$ is expressed by the difference of the phased structure factors:

$$\Delta\rho(\mathbf{r}) = \rho_a(\mathbf{r}) - \rho_b(\mathbf{r}) = \frac{1}{V}\sum_{\mathbf{H}} \Delta\mathbf{F}(\mathbf{H})\exp(-2\pi i\mathbf{H}\cdot\mathbf{r}) \quad (1)$$

with $\Delta\mathbf{F} = \mathbf{F}_a - \mathbf{F}_b$. If the phase of one set of structure factors is not known and the phase ϕ of the known set of structure factors is assigned to both sets, the residual density is obtained (Coppens, 1997):

$$\rho_0(\mathbf{r}) = \frac{1}{V}\sum_{\mathbf{H}} (F_a - F_b)\exp(i\phi_b)\exp(-2\pi i\mathbf{H}\cdot\mathbf{r}). \quad (2)$$

In dealing with the experimental residual density, the coefficients in $\Delta\mathbf{F}$ are $\mathbf{F}_{\rm obs}$ (the experimental structure-factor amplitudes) and $\mathbf{F}_{\rm calc}$ (those derived from a least-squares density model). In order for the Fourier summation to be independent of the X-ray frequency, it is normal in the calculation of the residual density according to equation (2) for the experimental structure factors $\mathbf{F}_{\rm obs}$ to be corrected for anomalous dispersion. Thus, even at this fundamental level of description, model-dependent entities may enter the field. The residual density given by (2) will be denoted ρ_0 throughout this paper. ρ_0 contains all sources of error and inadequacies of the modeling, like density model inadequacies and limitations (spherical atoms instead of non-spherical atoms, limitations in the basis set, non-relativistic scattering factors, only isotropic and harmonic U_{ij} *etc.*) as well as other sources of error like

inadequate data integration, wrong or inadequate correction for absorption, extinction and noise. The list is obviously not complete (Rollet, 1988).

The residual density defined according to equation (2) does not account for errors in the phase assignment. The maximum error possible in the phase assignment is π, which leads according to the more general equation (1) after a short calculation (see Appendix *A*) to a maximum error in the modulus of the difference structure factor of $|\Delta\mathbf{F}| = |F_{\rm obs} + F_{\rm calc}|$, whereas the maximum error in the residual density is, according to equation (2), $|\Delta\mathbf{F}| = |F_{\rm obs} - F_{\rm calc}|$. The difference is $2F_{\rm calc}$, which emphasizes the importance of phase contributions to the error. We are, however, concerned in this paper only with the contributions according to the residual density.

In X-ray diffraction experiments aiming at the reconstruction of the electron density in the unit cell, the parameters describing the electron density are obtained by a minimization of the weighted squared modulus of the difference between $F_{\rm obs}$ and $F_{\rm calc}$, or the respective modulus squared values, the intensities. The resulting fit is judged by the 'flatness' and the 'featurelessness' of the residual density. The first criterion is usually checked by a peak search revealing the highest peaks and the deepest holes of the residual-density distribution. In contrast, the 'featurelessness' of the resulting distribution is not quantified. In multipole models (MM) and maximum-entropy methods (MEM), it is tested by visual inspection of ρ_0 in certain planes containing the heaviest atoms. As all sources of error are present in the residual density, it might seem possible to analyze the residual-density distribution, not only for quality reasons but also for the diagnostic reason of finding the main source(s) of error present in a given refinement. This would open the way for systematic improvements in all fields connected to the description of electron densities (or momentum densities) in crystals. We call this process residual-density analysis and abbreviate it RDA. For this purpose, the residual density has to be characterized in detail, presenting the problem of how to assess the three-dimensional distribution in a convenient way, yet without loss of information. In this paper, we present new descriptors characterizing the total amount and the specific distribution of the residual density.

2.1. The multipole model (MM)

In the multipole density formalism according to Hansen & Coppens (1978), the molecular electron density is expanded in pseudo-atom density contributions. The density of each pseudo-atom is given by

$$\rho_{\rm at}(\mathbf{r}) = P_c\rho_{\rm core}(r) + P_v\kappa^3\rho_{\rm valence}(\kappa r) + \sum_{l=0}^{l_{\rm max}} \kappa'^3 R_l(\kappa' r) \sum_{m=0}^{l} P_{lm\pm} d_{lm\pm}(\theta,\phi) \quad (3)$$

with normalized radial density functions:

$$R_l(r) = \kappa'^3 \frac{\zeta^{n_l+3}}{(n_l+2)!}(\kappa' r)^{n_l}\exp(-\kappa'\zeta r) \quad (4)$$

and with real-valued normalized spherical harmonics:

$$d_{lm+} = N'_{lm}P_l^m(\cos\theta)\cos m\phi \quad (5)$$

$$d_{lm-} = N'_{lm}P_l^m(\cos\theta)\sin m\phi. \quad (6)$$

The $P_l^m(\cos\theta)$ are associated Legendre functions and N'_{lm} appropriately chosen normalization factors. In *XD* (Volkov *et al.*, 2006), it is also possible to use radial functions from a wavefunction in the data bank. The core density (P_c) is frozen. The multipole parameters to be refined are coordinates, population parameters P_v, P_{lm}, radial expansion/contraction parameters for monopoles (κ) and multipoles (κ'), and thermal-motion parameters U_{ij}.

2.2. The maximum-entropy method (MEM)

In applications of maximum-entropy methods to crystallographic problems, the electron density is reconstructed from diffraction data (Collins, 1982; Gilmore, 1996) by maximizing the entropy of the electron density in the unit cell:

$$S = -\sum_{k=1}^{N} \rho_k \ln(\rho_k/\tau_k), \quad (7)$$

where ρ_k is the value of the electron density at the kth grid point and τ_k is a reference density at the same grid point (prior). The maximization is subject to a normalization constraint

$$C_{N_{\rm el}} = N_{\rm el} - \frac{V_{\rm UC}}{N}\sum_{k=1}^{N}\rho_k = 0 \quad (8)$$

with $N_{\rm el}$ being the number of electrons, N the number of grid points, $V_{\rm UC}$ the volume of the unit cell, and with the additional constraint of fitting the diffraction data. This can be taken into account in different ways, *e.g.* according to the F_2 constraint (Sakata & Sato, 1990):

$$C_{F_2} = -1 + \frac{1}{N_F}\sum_{hkl} w_{\mathbf{H}}|F_{\rm obs}(\mathbf{H}) - F_{\rm MEM}(\mathbf{H})|^2 \quad (9)$$

with observed structure factors $F_{\rm obs}(\mathbf{H})$. $F_{\rm MEM}(\mathbf{H})$ is obtained by a discrete Fourier transform of the set of grid points $\{\rho_k\}$ and $w_{\mathbf{H}}$ is an appropriately chosen weight. N_F is the number of observed reflections. Other constraints also exist, for example the 'prior derived *F*-constraints' (Palatinus & van Smaalen, 2005).

The residual-density distribution is assumed to be Gaussian-like in the case of convergence, therefore a χ^2 test is employed. If the constraint approaches the expectation value $\langle C_{F_2}\rangle = 0$, ideally $\chi^2 = 1$ is expected.

3. Residual-density descriptors

For the characterization of residual distributions (in real space as well as in reciprocal space, *e.g.* for the investigation of residual momentum densities from density matrices), we suggest the use of the following descriptors.

3.1. Net residual electrons and net residual density

The number of net residual electrons is defined as the excess or missing number of electrons in a given volume of the unit

cell. It is derived by multiplication of the net residual density with the volume under consideration.

$$\rho_{\rm net} = \frac{1}{V}\int_V \rho_0(\mathbf{r})\,{\rm d}^3 r. \quad (10)$$

The index V at the integral sign emphasizes the dependence of the result from the volume chosen. For a residual-density grid, the integration becomes a summation over the grid points in the analyzed volume:

$$\rho_{\rm net} = \frac{1}{N}\sum_{k=1}^{N} \rho_0(k). \quad (11)$$

To obtain the net residual electrons, the volume has to be taken into account:

$$e_{\rm net} = \frac{V}{N}\sum_{k=1}^{N} \rho_0(k). \quad (12)$$

3.1.1. $e_{\rm net}$ and $\rho_{\rm net}$ as global descriptors. If the volume in equations (11) and (12) is chosen to be the volume of the unit cell, $e_{\rm net}$ and $\rho_{\rm net}$ must vanish:

$$\rho_{\rm net}(V_{\rm UC}) = e_{\rm net}(V_{UC}) \stackrel{!}{=} 0, \quad (13)$$

if the corresponding distributions ρ_a and ρ_b according to equation (1) comprise the same number of electrons. In this case, the integration of equation (2) over the unit cell yields zero. If one of the distributions, say ρ_b, is from a model density and the other distribution ρ_a is derived from the experimental $F_{\rm obs}$, the latter would be contaminated by noise and $e_{\rm net}$ calculated for the whole unit cell would quantify the amount of noise present. In real experiments, however, $F(000)$ is usually not measured and therefore it is excluded from the evaluation of equation (2). In consequence, the number of net residual electrons and the total net residual density must vanish for experimental data. In summary, the total number of net residual electrons for the whole unit cell provides a consistency check; it should be close to zero. The deviation from zero is a measure of the accuracy of the grid. As the values found for the whole unit cell were at most 10^{-6} e Å^{-3}, we will not list these numbers in the tables.

3.1.2. $e_{\rm net}$ and $\rho_{\rm net}$ as local descriptors. The global descriptor $e_{\rm net}(V_{\rm UC})$ turns into a local descriptor by summing only over a part of the unit cell. As in the hypothetical ideal case of a perfect model (and perfect data, see above), $e_{\rm net}$ would integrate to zero for *any* part of the unit cell, this local descriptor might also serve as an indicator for local weaknesses of the density model, such as inappropriate hydrogen-bonding distances, disorder, missing atoms or inappropriately parameterized pseudo-atoms. There are limits to the number of net residual electrons for a given volume: $-\rho_{\rm gross} \leq \frac{1}{2}\rho_{\rm net} \leq \rho_{\rm gross}$ and $-e_{\rm gross} \leq \frac{1}{2}e_{\rm net} \leq e_{\rm gross}$. To understand this, we need the definition of the gross residual electrons and gross residual density, which are to be defined in the next section. It can be said already, however, that, if in a given volume the ratio of net and gross residual electrons approaches the limiting value +2, a remarkable amount of density has not been modeled in this volume. This is for example the case in an unrefined disorder. An example for experimental data is given in §6.3.

3.2. Gross residual electrons and gross residual density

To quantify the total amount of (integrated) residual density, we suggest the use of the modulus of the residual-density distribution according to the following equations:

$$\rho_{\rm gross} = \frac{1}{2V}\int_V |\rho_0(\mathbf{r})|\,{\rm d}^3 r, \quad (14)$$

which translates on a discrete grid to

$$\rho_{\rm gross} = \frac{1}{2N}\sum_{k=1}^{N} |\rho_0(k)|, \quad (15)$$

where the summation runs over N grid points. The measure $\rho_{\rm gross}$ gives an average residual density. If equations (14) and (15) are multiplied by the volume under consideration, *e.g.* the volume of the whole or a part of the unit cell, one obtains the gross residual electrons:

$$e_{\rm gross} = \rho_{\rm gross} V. \quad (16)$$

This is a simple yet characteristic measure of the total amount of residual density present in that volume.

In the hypothetical case of an ideal model and ideal data (ideal: $F_{\rm obs} = F_{\rm calc}$ in a limited range of $\sin\theta/\lambda$), $e_{\rm gross}$ and $\rho_{\rm gross}$ are both zero independent of the volume chosen.

3.2.1. $e_{\rm gross}$ and $\rho_{\rm gross}$ as global descriptors. In contrast to $e_{\rm net}$, which vanishes for the whole unit cell, $e_{\rm gross}$ does not: if density is missing in any part of the unit cell, there must be some superfluous density in another part, provided all atoms have been identified correctly. Both regions increase the value of $e_{\rm gross}$. One misplaced electron generates in total a hole of 1 e in the region where the electron is missing, and a peak of 1 e in the region where it was artificially placed; therefore, one misplaced electron generates 2 e out of place. This is the reason for the factor 1/2 in the above equations. Choosing V to be the volume of the unit cell, the gross residual density is in proportion to an average residual density. The gross residual electrons describe the total inadequacies arising from noise (see §5.2), inadequate data processing (see §6.4) and density model errors (see §§5.4, 5.5, 6.3). It will be shown that $e_{\rm gross}$ is grid independent (§6.1) as possibly expected from the grid-size independence of R values, which also describe the total error present in a refinement. The value of $e_{\rm gross}$ can artificially be lowered by truncation of the experimental resolution (§5.1).

3.2.2. $e_{\rm gross}$ and $\rho_{\rm gross}$ as local descriptors. Improving the density model leads to a reduced value for $e_{\rm gross}$ (§6.3). Neglecting data processing errors, the total number of gross residual electrons is therefore determined by the contributions from noise, which cannot be described in multipole models but in MEM, and model errors: $e_{\rm gross} = e_{\rm gross,n} + e_{\rm gross,me}$ (n: noise, me: model errors). This result leads to the requirement of minimum gross residual electrons for the best multipole density model since this leaves only the gross residual electrons due to noise, which is inherent to the data. This is of

particular importance in MM as, for example, the radial scaling parameters, κ', may be highly correlated with other parameters and, as a result, convergence becomes difficult when refined together with all other parameters. Therefore, the process has to be stopped at some point or the κ' refinement has to be done independently of the other parameters. But then the stability of the model, which is usually proven by a common final refinement of all parameters, is not given and bias may be introduced by the block refinement. In this case, $e_{\rm gross}$ can be helpful to identify too diffuse electron-density distributions by a local evaluation of $e_{\rm gross}$ in a volume containing the atoms under consideration.

3.3. The fractal dimension distribution of the residual density

3.3.1. Motivation. $e_{\rm gross}$ [equation (12)] and $e_{\rm net}$ [equation (16)] quantify the basic requirement of a balance of positive and negative values and the total amount of ρ_0 present.

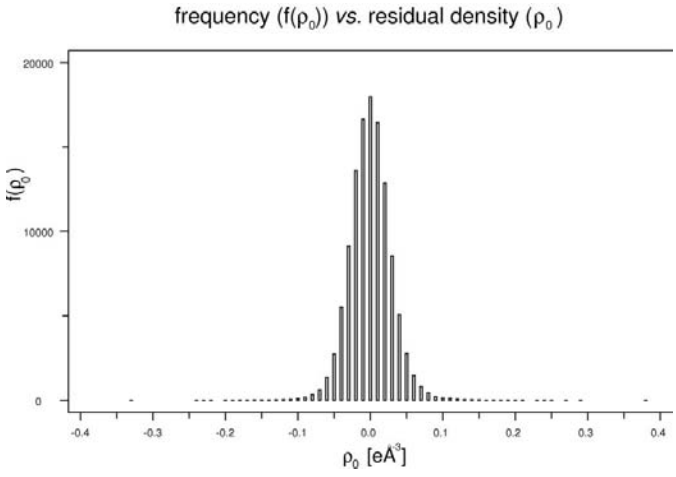

Figure 1
Histogram of the residual density of a multipole refinement on $S(N^tBu)_3$. The distribution does not show any special features.

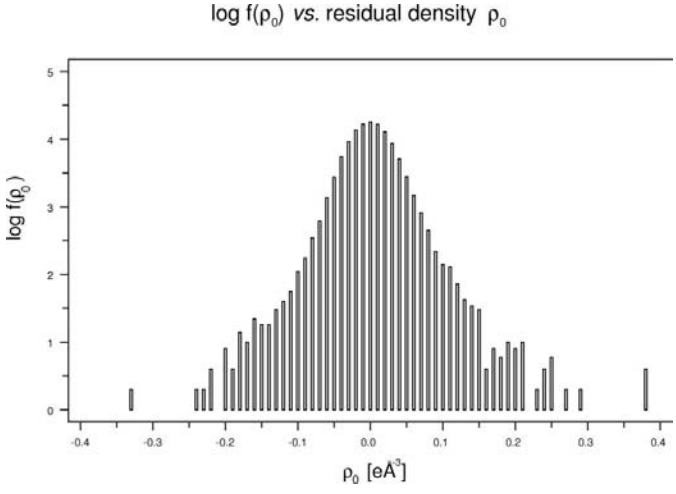

Figure 2
The histogram of Fig. 1 plotted on a logarithmic scale.

Nothing has been stated about the detailed distribution so far. For investigating the distribution of ρ_0, we first have to think about the requirements that have to be obeyed by the residual-density distribution. It is commonly anticipated and it can be derived from the Poisson process of the intensity measurement and the central limit theorem that a Gauss function is a valid approximation to the distribution of residuals if no systematic error is present (French & Wilson, 1978). This helps us to define features in the residual density. The residual density is *not* featureless if its distribution is not reminiscent of a Gauss distribution. The reverse is not true as, to an overall perfect residual density of zero everywhere in the unit cell, a Gaussian error distribution could be added 'by hand', yielding *e.g.* a Gaussian residual-density distribution and an obvious error. Please note that according to this definition of features a least-squares refinement does not minimize the features in the residual density but only its flatness.

A simple approach to investigate the residual-density distribution is to calculate a histogram and compare it to a Gaussian distribution, *e.g.* by means of a χ^2 test or by visual inspection. As an example, see Fig. 1, which shows the residual-density histogram for a refinement on $S(N^tBu)_3$ (Leusser *et al.*, 2004).[1] Owing to the high frequency of residual-density values close to zero, details in the periphery cannot be observed easily. Therefore, it might be helpful to take the logarithm of the histogram (Fig. 2). It is more obvious now that the residual-density distribution does not follow a Gaussian distribution, in which case the plot on a logarithmic scale would be a parabola. The plot shows deviations from the parabolic shape in particular in the periphery, *i.e.* for the large values of the (modulus of the) residual density. This is a sign of the presence of systematic errors. We will find an interpretation for this systematic error later. At present, just a part of the goal is achieved. The log-histogram plot shows systematic errors in detail but no meaning is given to the values of the residual density. What, for instance, is the relevance of the maximum value of approximately 4.3 in the log-histogram plot? Can we go one step further and assign a meaning to these values and in this way bound the spectrum of values to a reasonable range? This can be achieved in the fractal dimension approach, which will be developed in the next paragraphs. A fractal dimension plot of the same residual density is depicted in Fig. 3. In this approach, there is an upper

[1] Later there follows an application to experimental data. We give the full details of the measurement and crystallographic data here. Measurement: The data were collected in ω-scan mode from shock-cooled crystals using graphite-monochromated Mo $K\alpha$ radiation ($\lambda = 0.71073$ Å) at 100 (2) K. Data collections were performed in two independent batches, a low-angle ($2\theta_{\rm detector} = -31^\circ$) and a high-angle batch ($2\theta_{\rm detector} = -80^\circ$), respectively. The resulting data sets were assigned an individual scaling factor and were treated independently during all steps of data processing. The small overlap region was not employed to scale both batches. This strategy allows a maximum resolution limit of up to $\sin\theta/\lambda = 1.14$ Å^{-1} from only two batches of data. Crystallographic data: $C_{12}H_{27}N_3S_1$, $M = 245.43$, triclinic, space group $P\bar{1}$, $a = 9.3228$ (3), $b = 9.3455$ (3), $c = 10.6675$ (3) Å, $\alpha = 70.5150$ (10), $\beta = 77.5710$ (10), $\gamma = 60.5540$ (10)°, $V = 761.52$ (4) Å^3, $Z = 2$, $\rho_{\rm calcd} = 1.070$ Mg m^{-3}, $\mu = 0.196$ mm^{-1}, $F(000) = 272$, 17996 reflections measured (low-angle batch, $\sin\theta/\lambda < 0.625$ Å^{-1}), $R_{\rm int} = 0.0287$, 44864 reflections measured (high-angle batch, $0.625 < \sin\theta/\lambda < 1.140$ Å^{-1}), $R_{\rm int} = 0.0307$, 18250 unique reflections.

limit to the 'frequency' of the residual-density values of 3. Like in the log-histogram plot, the difference from the ideal Gaussian distribution shows up as deviation from the parabolic shape.

For motivating the fractal dimension approach, let us consider three hypothetical limiting cases to discuss the implications for the residual-density distribution, in particular for the iso-surface of constant residual density $\rho_0(\mathbf{r}) = 0$ e Å^{-3}. This value is chosen because it is particularly easy to discuss and since the least-squares refinement tries to produce as much zero residual density as possible. These hypothetical cases are a *gedanken* experiment: a laboratory for developing ideas. In the applications of the developed concepts, the highly idealized assumptions of the *gedanken* experiment need not be realized.

In the first case, we assume that the data are free from noise and errors and that the density model is perfect in a least-squares sense, *i.e.* the $F_{\rm calc}$ reproduce exactly the $F_{\rm obs}$ in the observed set of structure factors. Please keep in mind that this is just a *gedanken* experiment. A limited resolution is assumed.

This highly idealized situation clearly results in $\rho_0(\mathbf{r}) \equiv 0$ e Å^{-3} for all $\mathbf{r}$ in the entire unit cell. The distribution is absolutely flat and it is featureless because of the complete homogeneity. This distribution topologically constitutes a three-dimensional manifold and both $e_{\rm gross}$ and $e_{\rm net}$ are zero.

In the second hypothetical case, the assumption of a perfect model is made but the data now contain random (Gaussian) noise. It is assumed that the amount of noise can be characterized by a noise control parameter p_1. In this case, $\rho_0(\mathbf{r}) = 0$ e Å^{-3} cannot hold true any more for the entire unit cell. There will be regions of positive and negative residual-density values, separated by surfaces of zero residual density. The minimum, $\rho_{0,\rm min} \neq 0$ e Å^{-3}, and the maximum residual-density values, $\rho_{0,\rm max} \neq 0$ e Å^{-3}, are of approximately the same absolute value. The difference $\Delta\rho_0 = \rho_{0,\rm max} - \rho_{0,\rm min}$ quantifies the flatness of the distribution. The union of iso-surfaces of zero residual-density value covers an area that can be expressed in multiples of the unit area, which is, after rescaling the unit cell to the unit cube, the characteristic area of the system. In the case of many highly curved iso-surfaces of constant $\rho_0(\mathbf{r}) = 0$ e Å^{-3}, the resulting area can exceed the unit area by a large factor. In this case, the topological surface under consideration becomes almost space-filling. The word 'almost' is crucial as it indicates that the dimension of the manifold under consideration may be expressed by a non-integer number close to but smaller than 3. Non-integer dimensional values are well known from the area of mathematics called fractal geometry that deals with the dimensions of irregularly shaped natural objects like plants, trees, mountains and coast lines or 'strange' mathematical objects like the Koch curve (see *e.g.* Bronstein *et al.*, 1993, and references cited therein). The assigned number is called the 'fractal dimension', 'Hausdorff dimension', sometimes also 'Hausdorff–Besicovitch dimension' or 'Mandelbrot dimension'. The definition of the fractal dimension, which will be abbreviated d^f, follows in the next section. Since in our second hypothetical case there is no structural information present in the residual density, the number $d^f(\rho_0 = 0) = d^f(0) < 3$ gives an upper limit for the best possible model. In this respect, it characterizes the data and marks the convergence limit for the perfect model. The number of gross residual electrons will be greater than zero; it quantifies the total amount of noise present in the data.

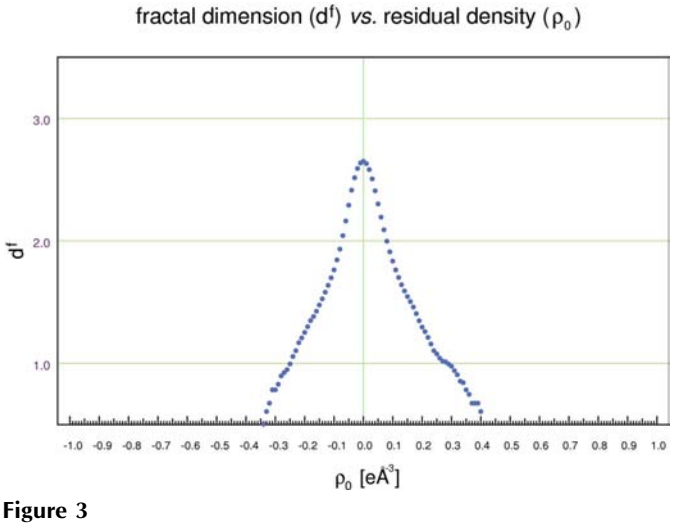

Figure 3
The fractal dimension distribution of the residual density underlying Figs. 1 and 2.

In the third hypothetical case, the data as well as the model are imperfect, thus introducing random noise and bias. As in the preceding example, $\Delta\rho_0 \neq 0$ e Å^{-3}. The imperfections of the model create regions of excess/missing density. In this way, the dimensionality of the iso-surface $\rho_0 = 0$ e Å^{-3} (*i.e.* the number of grid points in the residual-density grid with value zero) will be further reduced if the typical extension of the newly introduced regions is on average larger than typical extensions of residual-density 'bubbles' arising due to the noise. The reduction is a measure of model bias. The number $e_{\rm gross}$ describes noise in the data and model bias. If the amount of noise characterized by p_1 is the same as in the example before, then $e_{\rm gross}$ will be increased. This follows from the additivity $e_{\rm gross} = e_{\rm gross,n} + e_{\rm gross,me}$, where $e_{\rm gross,n}$ are the gross residual electrons due to noise and $e_{\rm gross,me}$ are those due to model errors.

3.3.2. The fractal dimension distribution of the residual density. The fractal dimension of a residual-density iso-surface of constant value x is defined according to Bronstein *et al.* (1993):

$$d^f(\rho_0 = x) = \lim_{\varepsilon \to 0} \frac{\log N(x, \varepsilon)}{\log(1/\varepsilon)}, \qquad (17)$$

where ε is the characteristic length of a box covering the manifold under consideration, and $N(x, \varepsilon)$ is the number of boxes a desired value x was present in. If the manifold is exhaustively covered by disjoint boxes of the same length ε, equation (17) may be used to evaluate the fractal dimension on a finite grid, this is then called a box-counting algorithm (Bronstein *et al.*, 1993). If one is interested in, say, the zero residual-density iso-surface, one just counts the number of

boxes $N(\varepsilon)$ containing at least one point of zero residual density. The result is dependent on the edge length ε of the boxes. In the limit $\varepsilon \rightarrow 0$, the result converges against the area of this surface. The power law underlying equation (17) describes how fast the number of boxes increases when the box length decreases:

$$N(\varepsilon) \propto \varepsilon^{-d^f}. \tag{18}$$

For a three-dimensional object, the number of boxes increases with the third power of the inverse box length, thereby assigning the dimensional value 3 to this body. If, however, not the whole space is filled with the manifold, the dimensionality in the sense of the fractal dimension may reduce to a value smaller than 3. For a two-dimensional object, squares would be taken instead of boxes and the number of squares would increase according to ε^{-2}. If the manifold does not cover the whole plane, the dimensionality in terms of the fractal dimension may reduce to a value smaller than 2. Natural fractals like dendritic structures, trees, coast lines, the surfaces of human brains and the residual-density distribution are not scale-invariant on all scales like pure mathematical fractals, which are constructed by an infinite iterative application of a generator acting on a starting manifold. If this process is stopped, the actual result is a pre-fractal. Nevertheless, the fractal nature of the distribution exists on a limited scale and it can be adequately described by a box-counting algorithm with finite edge length ε. In the special case of a distribution containing Gaussian noise with a mean of zero, $N(\rho_0, \varepsilon) \propto \exp(-\rho_0^2/2\sigma^2)$, and no model errors, it follows from equation (17) that the corresponding fractal dimension distribution is of parabolic shape, with a maximum value of $d^f(0) = 3$. At this limit, the parabola degenerates to a single point.

It will be seen later that $d^f(\rho_0)$ is dependent on the residual-density grid (§6.1). $d^f(0)$ is connected to the experimental resolution (§5.1), noise (§5.2), density model errors (§6.3) and data processing inadequacies (§6.4). In consequence, for a fixed number of grid points n_x, n_y, n_z and given experimental data, $d^f(0)$ depends solely on the density model. Therefore, it can be used as a measure for the featurelessness of the residual-density distribution.

4. Software implementation

Software called *jnk2RDA* has been written which evaluates a residual-density grid as given by the Fourier programs *XDFOUR* or *XDFFT*, which are part of the *XD* program package. The software calculates the descriptors $e_{\rm gross}$, $e_{\rm net}$ and the distribution $d^f(\rho_0)$ for the whole range $\rho_{0,\rm min} \leq \rho_0 \leq \rho_{0,\rm max}$, the positive and negative residual-density values for which $d^f(\rho_0) = 2$ are also given. This value is virtually grid independent and very moderately affected by model errors, thus it may serve as a measure of noise. The value $d^f(\rho_0) = 2$ will be discussed later. Output is provided in the form of a PostScript file showing the distribution $d^f(\rho_0)$ in steps of 0.01 e Å^{-3} in the standard residual-density range from -1 to $+1$ e Å^{-3} and some additional information read in from the xd.mas file. The fractal dimension distribution of the residual-density grid is evaluated by a line-counting algorithm (instead of a box-counting algorithm), which implementation is now described in detail.

Let us assume that we wish to compute the fractal dimension at n chosen residual-density levels between $\rho_0 = -1.0$ and $\rho_0 = +1.0$ e Å^{-3} for a three-dimensional grid file $\rho_0(i, j, k)$ which has n_x, n_y, n_z points along the respective axes. We simply check whether the iso-surface for each of these n chosen points in ρ_0 intersects the line defined by consecutive pairs of points $\rho_0(i, j, k)$ and $\rho_0(i + 1, j, k)$ in the grid file, *i.e.* whether the value of ρ_0 at each residual-density level n_i lies between the values spanned by $\rho_0(i, j, k)$ and $\rho_0(i + 1, j, k)$. Each time the value n_i satisfies this condition, the count in the bin for n_i is incremented by one. This line counting along all $n_y \times n_z$ lines in the x direction is then repeated for all $n_x \times n_z$ lines in the y direction and all $n_x \times n_y$ lines in the z direction.

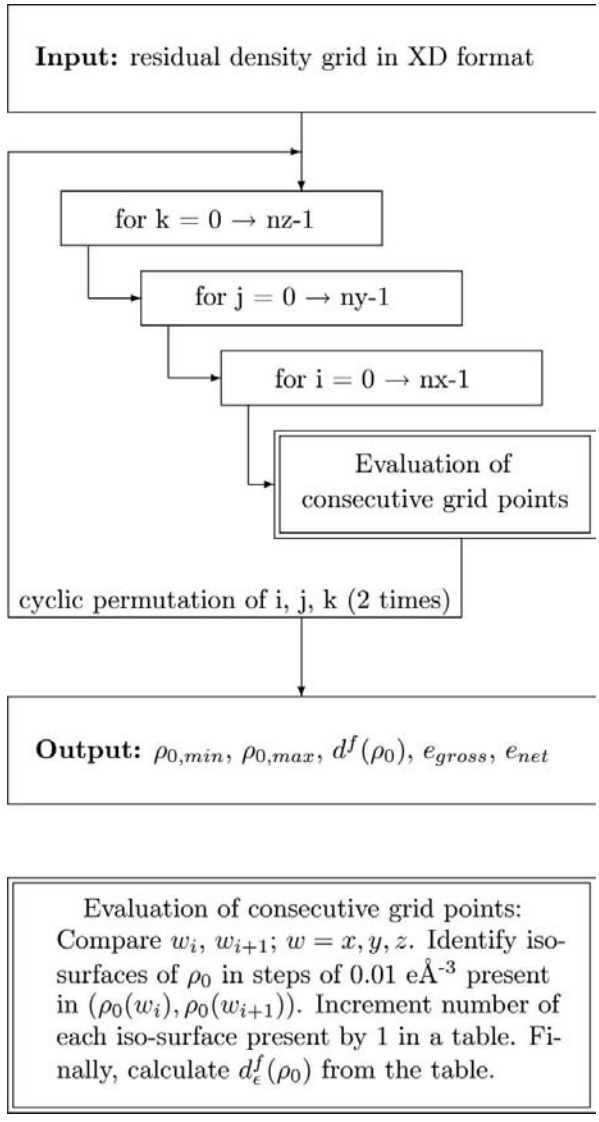

Figure 4
Schematic representation of the calculation process.

Table 1
The fractal dimension of $\rho_0 = 0$ e Å^{-3} for simulated noise-free data ($p_1 = 0$) for S(N^{t}Bu)$_3$ with increasing resolution.

The $\mathbf{F}_{obs}$ were calculated from a multipole model for the indicated resolution. $|\rho_0| \leq 0.01$ e Å^{-3} for all resolutions. The last column gives the predicted values from a linear regression (l.r.) according to the equation $d^f(0) = a + bd$ with constant parameters a, b and resolution d. $a = 2.90392$, $b = -0.462513$, $R^2 = 0.996707$.

$\sin\theta/\lambda$ (Å^{-1})	d (Å)	$d^f(0)$	l.r.
0.80	0.63	2.61	2.61
0.90	0.56	2.65	2.65
1.00	0.50	2.67	2.67
1.14	0.44	2.70	2.70
1.30	0.38	2.73	2.73
1.50	0.33	2.75	2.75

The characteristic length ε in (17) is given by the cube root of the reciprocal of the total number of pairs of grid points examined, or by the square root for a two-dimensional grid.

A diagrammatic representation of this algorithm is given in Fig. 4. The evaluation of a $50 \times 50 \times 50$ residual-density grid typically takes a few seconds. The results are similar to the box-counting algorithm, *i.e.* the plots are very similar in shape but differ in detail, particularly in $d^f(0)$. Other ways for the evaluation of d^f based on binning techniques have been tested, too. The line-counting procedure, however, is faster than the box-counting algorithm and more exact than binning techniques. Binning techniques are extremely fast but need additional parameters like the bin width, which has to be determined dynamically and influences the result significantly. Moreover, the binning of values gives no guarantee that certain levels are present at all. This leads to an incorrect result in particular for the very small and the very large values. The box-counting algorithm implemented led to very similar shapes in the residual-density distribution but with values positively shifted in comparison to the line-counting algorithm. In a case study, this shift in d^f was found to be systematically close to 0.2. That different algorithms may lead to different values in the fractal dimension determination has already been described in the literature (Brewer & Di Girolamo, 2006). It is therefore indispensable to decide on the algorithm to use and then maintain this choice as otherwise the values are not comparable. We decided to use the line-counting algorithm as it is faster and more efficient than the box-counting algorithm.

5. Application to simulated data

5.1. Experimental resolution

For investigating the influence of the resolution on $d^f(0)$, a number of ideal noise-free structure-factor data sets (h, k, l, I) for the molecule S(N^{t}Bu)$_3$ was calculated for different resolutions from the completely converged multipole refinement on experimental data. Initial structure factors were calculated with *XPREP* (Bruker, 2006) for the desired resolution and were subsequently replaced by the $|F_{calc}|^2$ calculated by *XDLSM* to obtain ideal structure factors from aspherical pseudo-atoms (Table 1). The residual-density files were generated with *XDFOUR* for a range $0.8 \leq (\sin\theta/\lambda)_{max} \leq 1.5$ Å^{-1} after application of ten cycles of least-squares refinement of all parameters with *XDLSM*. The modulus of the residual density is smaller than 0.01 e Å^{-3}. $d^f(\rho_0)$ increases steadily with the resolution from $d^f(0) = 2.61$ to 2.75, *i.e.* although neither noise nor model errors are present the value $d^f(0) = 3.0$ is not reached. We interpret the difference to $d^f(0) = 3$ as the spatial correlation of consecutive residual-density values to have the same sign, as only a change of the sign contributes to $d^f(0)$ in the applied line-counting algorithm. In consequence, the numerical value of $d^f(0)$ should depend not only on the experimental resolution but also on the grid spacing, which is indeed the case (see §6.1).

5.2. Gaussian noise

Noise was added to the simulated structure factors [for the procedure to obtain ideal noise-free structure factors with an R_2 factor as defined in *XD* ($R_2 = \sum |F_o^2 - F_c^2| / \sum |F_o^2|$) typically smaller than 0.02% see the preceding paragraph] by addition of an error intensity distributed according to a Gaussian probability density function (random Gaussian noise, abbreviated RandomGN) with an expectation value $\langle I_{hkl}^{error} \rangle = 0$ and a standard deviation σ proportional to the square root of the intensity:

$$
\begin{aligned}
I_{hkl}^{noise} &= I_{hkl}^{ideal} + I_{hkl}^{error} \\
I_{hkl}^{error} &= p_1 \sqrt{I_{hkl}^{ideal}}\,\mathrm{RandomGN}(\mu, \sigma) \\
\mathrm{RandomGN}(x) &= \frac{1}{\sqrt{2\pi}\sigma} \exp\left(-\frac{(x-\mu)^2}{2\sigma^2}\right) \\
\sigma &= 1 \\
\mu &= 0,
\end{aligned}
\qquad (19)
$$

with an adjustable noise control parameter $0 \leq p_1 \leq 1$. The probability $p(x)\,\mathrm{d}x$ of adding an error in the small range $(x, x + \mathrm{d}x)$ close to x is $p(x) = (1/\sqrt{2\pi}\sigma) \exp[-(x-\mu)^2/2\sigma^2]$, which leads by integration from $-\sigma$ to σ to a value of approximately 68.3% for the range $-\sigma \leq x \leq \sigma$.

As the SKIP option was used to exclude negative intensities from the refinement, the procedure described leads to a bias, which, however, may be small for small values of p_1, since in this case only very rarely are negative total intensities created. A Perl script was written to add I_{hkl}^{error} to I_{hkl}^{ideal} according to equations (19) and write a new xd.hkl file. Ten cycles of least-squares refinement of all parameters were performed with *XDLSM*, followed by a Fourier synthesis with *XDFOUR*. The resulting distributions of the fractal dimension for the simulated data are depicted in Fig. 5 and the corresponding descriptors including those for the experimental data are listed in Table 2. Setting $p_1 = 0$, *i.e.* adding no noise, results in a single point at $d^f(0) = 2.70$. We interpret this number as an upper limit for $d^f(0)$, which could be reached if noise in the experimental data was absent for the given resolution.

Table 2
Residual-density descriptors applied to simulated noisy data (resolution 1.14 Å^{-1}) for S(N^{t}Bu)$_3$ with increasing noise.

Ten cycles of least-squares refinement with *XDLSM* were applied after addition of noise. For a graphical representation, see Fig. 5. Grid points: 93 × 93 × 107. For comparison, the descriptors for experimental data are also given.

p_1	$d^f(0)$	$\Delta\rho_0$ (e Å^{-3})	$e_{\rm gross}$ (e)
0.000	2.70	<0.01	0.31
0.222	2.68	0.25	8.29
0.444	2.67	0.50	16.20
0.888	2.67	0.93	30.60
Experiment	2.65	0.74	8.38

Table 3
Residual-density descriptors applied to simulated noisy data for S(N^{t}Bu)$_3$ to study truncation effects.

The noise control parameter was set to $p_1 = 0.222$. The truncation was applied only to the calculation of the residual-density grid, while the density parameters (multipole parameters, U_{ij}, x, y, z) were obtained from a refinement on the full data range. A 93 × 93 × 107 grid was used. See also Fig. 6.

$(\sin\theta/\lambda)_{\rm max}$ (Å^{-1})	$d^f(0)$	$\Delta\rho_0$ (e Å^{-3})	$e_{\rm gross}$ (e)
1.14 (theory)	2.68	0.25	8.29
0.80 (theory)	2.61	0.13	4.92
1.14 (experiment)	2.65	0.74	8.38

Increasing the noise level to $p_1 = 0.222$, such that the experimental value of $e_{\rm gross} \approx 8.4$ is approximately met, one finds a small reduction of the maximum value in the distribution to $d^f(0) = 2.68$, giving an upper limit for any reasonable density model. For a multipole model, due to its noise averaging properties (*i.e.* due to the noiseless model), this would be an upper limit, while for a maximum-entropy approach due to its ability to absorb noise into the density model it would not represent a limiting value but a target figure. The flatness is $\Delta\rho_0 = 0.25$ e Å^{-3} and $e_{\rm gross} = 8.3$ e, quantifying the amount of noise present. In summary: noise broadens the shape of $d^f(\rho_0)$, increases $e_{\rm gross}$ and $\Delta\rho_0$, and reduces the attainable featurelessness to the value $d^f(0)_{p_1>0} < d^f(0)_{p_1=0}$. Interestingly, contaminating the structure factors with increasing noise increases $e_{\rm gross}$ and $\Delta\rho_0$ proportionally, but $d^f(0)$ quickly seems to remain stable at $d^f(0) \approx 2.67$ (see Table 2). This is surprising as increasing the noise by a factor k might lead to the assumption that effectively only the residual density is multiplied by the same factor k. Note, however, that the density parameters were refined after addition of noise and that negative Fourier components are omitted. These occur mainly in the high-frequency range. Therefore, adding noise on the intensities effectively truncates the data. Truncation of data, in turn, leads to the initial decrease in $d^f(0)$.

5.3. Truncation of the resolution

Truncation of the resolution smoothes the residual density. Therefore, in publications it is sometimes found that the resolution for calculation of the residual-density plots and for the parameter determination are different. This is of particular importance if the molecules contain heavy atoms, since in the vicinity of heavy atoms large residual-density peaks or holes occur if the residual density is calculated for the full experimental resolution. This procedure is inconsistent in at least two ways. Firstly, the least-squares refinement of the density-model parameters is dependent on the data used. Therefore, all procedures following the density-model-parameter determination should be carried out at the same resolution for the sake of consistency. If the density-model parameters were

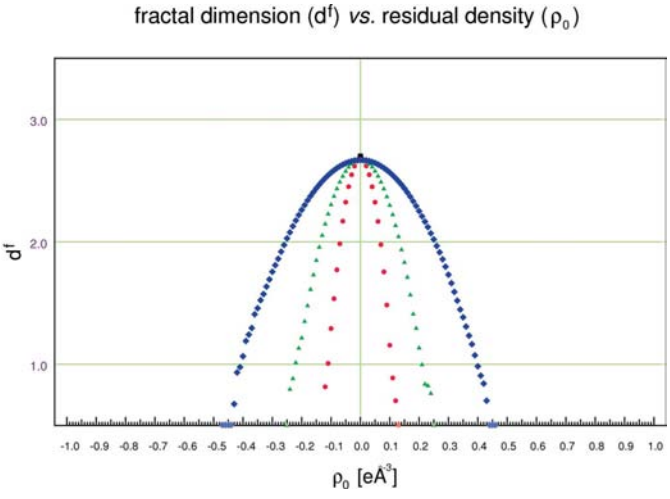

Figure 5
Residual-density descriptor $d^f(\rho_0)$ and noise: simulated data of S(N^{t}Bu)$_3$ for $\sin\theta/\lambda = 1.14$ Å^{-1}. Black filled square: $p_1 = 0.000$. Red filled circles: $p_1 = 0.222$. Green filled triangles: $p_1 = 0.444$. Blue filled diamonds: $p_1 = 0.888$. For more information see text and Table 2.

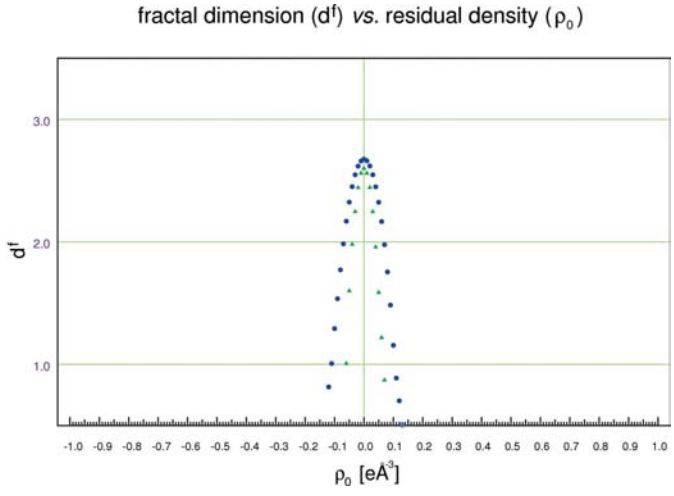

Figure 6
Truncation effects in $(\sin\theta/\lambda)_{\rm max}$ for simulated data with a noise level at $p_1 = 0.222$ for S(N^{t}Bu)$_3$. Blue filled circles: $(\sin\theta/\lambda)_{\rm max} = 1.14$ Å^{-1}. Green filled triangles: $(\sin\theta/\lambda)_{\rm max} = 0.80$ Å^{-1}. The truncation leads to a decrease in flatness to $\Delta\rho_0 = 0.13$ e Å^{-3} and to a reduction of $d^f(0)$ by about 0.07. The total error as given by $e_{\rm gross}$ decreases by 3.37 e. See also Table 3.

Table 4
Residual-density descriptors applied to simulated noisy data for $S(N^tBu)_3$ to study the effect of density-model errors on the residual-density descriptors.

The noise control parameter was set to $p_1 = 0.222$. s_0 is the unchanged scale factor, κ_0 is the unchanged radial screening parameter for the S atom. After modification of the scale factor, no refinement was applied. The scale factor was exclusively refined after modification of κ. See also Figs. 7, 8.

	$d^f(0)$	$\Delta\rho_0$ (e Å^{-3})	e_{gross} (e)
1.002 s_0	2.68	0.40	8.32
0.95 κ_0	2.67	0.38	8.56

determined at the reduced resolution, the parameters would be different from those of the untruncated data. The parameter values for the complete data set cannot be derived from the truncated data set. Secondly, in high-resolution X-ray studies aiming at the detailed reconstruction of the electron density, it is not helpful to artificially neglect the high-frequency Fourier components, where these generate chemically uninterpretable features and at the same time discuss fine topological details like the density and Laplacian at certain points, calculated from the whole data set. An evaluation of the residual-density descriptors after truncation of simulated data on $S(N^tBu)_3$ shows (see Table 3 and Fig. 6) that the residual density becomes flat, indeed $\Delta\rho_0$ decreases from 0.25 to 0.13 e Å^{-3}. Also, $d^f(0)$ decreases, as might be expected from the resolution dependence of $d^f(\rho_0)$. Simultaneously, however, also e_{gross} decreases from 8.29 to 4.92 e. The interpretation of e_{gross} as a measure of all errors and inadequacies made now shows that there is a 'progress' of over three gross residual electrons (this is the order of magnitude a multipole refinement on the same data achieves, see §6.3) without changing the density model or the data processing, *i.e.* these gross residual electrons just disappeared. Obviously, this progress is only cosmetic.

5.4. Model errors: scale factor

In a further study employing simulated data, the effect of model errors is evaluated. First, the scale factor was slightly increased by 2 per thousand, while all other parameters were kept fixed. The results are depicted in Fig. 7 and described in detail in Table 4. For comparison with the unaltered parameters, see Table 2, second row. A flat shoulder in the negative residual-density regime is typical for an erroneously increased scale factor. The interpretation is trivial: increasing the scale factor leads to a (on average) negative difference $F_{obs} - sF_{calc}$ (s scale factor) and therefore to a shoulder in the negative residual-density periphery. In consequence, a similar shoulder appears in the positive part of the residual density if the scale factor is decreased. This small numerical change in the scale factor increases $\Delta\rho_0$ substantially from 0.25 to 0.40 e Å^{-3}. Also, e_{gross} is increased from 8.29 to 8.32 e, which is the same order of magnitude as the error in the scale factor. In contrast to the aforementioned descriptors, $d^f(0)$ changes only very little (decrease in the fourth decimal place). It has been mentioned earlier that also distinct errors in the density model, like the errors corresponding to an independent-atom model (IAM), affect $d^f(0)$ only moderately.

5.5. Model errors: κ refinement

In contrast to the scale factor, which applies to all structure factors in the same way, the radial screening parameter κ can be chosen for each atom individually. To test the effect of small errors in κ, we deliberately fixed it for the S atom at a value slightly deviating from the optimum value, *i.e.* κ was decreased by 5% and a residual-density grid was calculated without

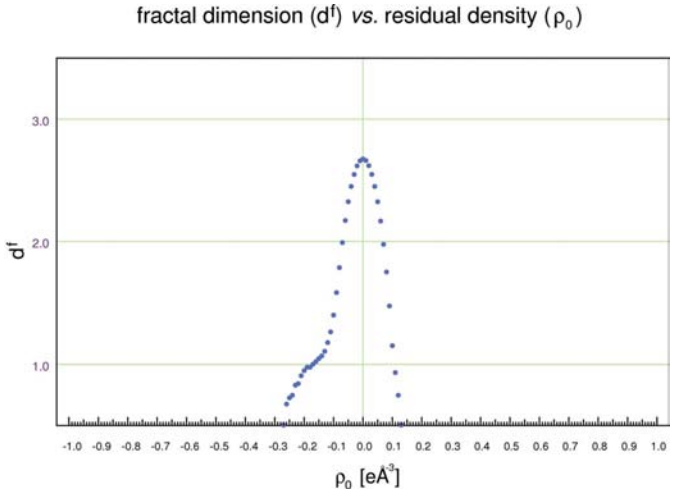

Figure 7
Model errors added to simulated data for $S(N^tBu)_3$ at a noise level of $p_1 = 0.222$. The scale factor has been changed slightly from 1.00041000 to 1.00241082 while all other parameters remain the same. The flat shoulder appears in the positive residual-density regime if the scale factor is decreased.

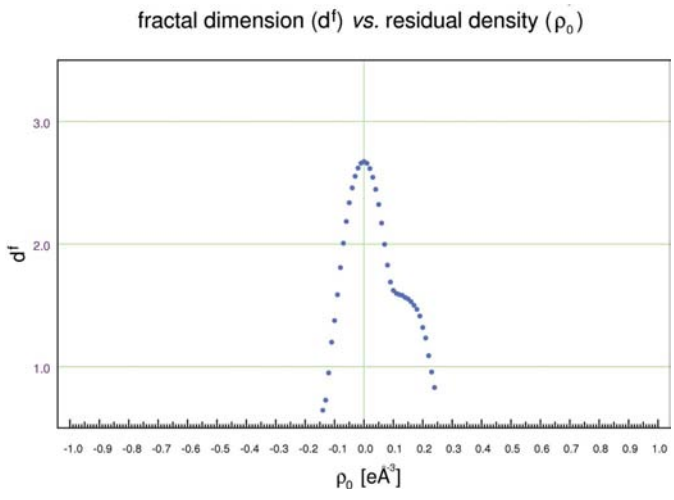

Figure 8
Model errors added to simulated data for $S(N^tBu)_3$ at a noise level of $p_1 = 0.222$. The radial screening parameter κ was changed for the S atom from 1.093200 to 1.038540 while all remaining parameters except for the scale factor were held constant. The shoulder appears in the negative residual-density regime if κ is increased instead of decreased.

changing any other parameters, but allowing the scale factor to change (*i.e.* the option CYCLE was set to −1 in *XDLSM*). The results are listed in Table 4 and depicted in Fig. 8, which this time shows a distinct shoulder on a higher-dimensional level than before and in the positive residual-density regime. A decrease of κ leads locally to a spatially more extended $\rho(\mathbf{r})$ in the vicinity of the S atom and to a very compact region at the nucleus with decreased $\rho(\mathbf{r})$. Because of the high density of electrons near the nucleus, a decreased $\rho(\mathbf{r})$ has a much higher impact on the residual density than has the increase in the region further away from the nucleus. Thus, the positive residual density at the nucleus results in a distinct shoulder in the positive residual-density regime in Fig. 8, whereas the increase in negative residual density is negligible. In the example with the scale factor, the error in the residual density is spatially more equally distributed such that each individual grid point contributes to only one or even none of the residual-density levels.

6. Application to experimental data

To demonstrate the practical applicability and usefulness of the descriptors, we applied these to truncated experimental data (§6.2), to the individual steps of an experimental multipole refinement (§6.3), to residual density from an IAM employing experimental data which was (was not) corrected for extinction (§6.4) and we studied how noise can be separated from structural information (§6.5). First of all, however, an analysis of the influence of the spatial grid resolution on the residual density descriptors is given.

6.1. Spatial grid resolution

To investigate the dependence on the spatial resolution, the residual-density grid was calculated for the fully converged multipole model on experimental data for $n_x \times n_y \times n_z = (50^3, 100^3, 200^3, 500^3, 750^3, 1000^3)$ grid points, *i.e.* the density model and the experimental data as well as the experimental resolution are fixed at constant values. The fractal dimension $d^f(0)$ decreases monotonically with increasing resolution (see Table 5 and Fig. 9) whereas in the periphery $d^f(\rho_0)$ is monotonically increasing. The negative and positive residual-density values for which the fractal dimension is equal to 2 remain almost unchanged. The flatness as given by $\Delta\rho_0$ decreases and $e_{\rm gross}$ is constant. The interpretation is as follows: two convergence processes take place, *i.e.* the residual-density values on the grid and the $\varepsilon \rightarrow 0$ convergence according to equation (17). Only for a grid of 500^3 points is the residual density essentially converged as can be seen from the constant value for $\Delta\rho_0$. The changes in $d^f(0)$ are much smaller then, too: they decrease from $\Delta d^f(0) = 0.0790$ to 0.0285 and finally to 0.0183 for the differences from 500^3 and 200^3, from 750^3 and 500^3 and from 1000^3 and 750^3 grid points, respectively. The smaller ε gets, the more detailed is the residual-density description and the less spatial averaging is introduced, as the value of the residual density at a given grid point approaches the average value for the volume associated with that grid point for the limit of vanishing ε. Note that any kind of averaging reduces the modulus of the local maxima and minima of this function, hence the decreased flatness for the coarse grid. The plot (Fig. 9) shows that the error in the dimensionality distribution is dominated by this averaging error: after convergence of the residual density for the 500^3 grid, the changes are generally very small. The same averaging error also explains why the fractal dimension is always underestimated in the periphery, whereas the dimensionality close to zero is overestimated: a coarse grid overestimates the contribution from frequent events like those close to $\rho_0 = 0$ e Å^{-3} by assigning an overestimated volume to each of these events. This must hold for the periphery, too, however, the suppresion of extreme values due to spatial averaging still dominates.

Table 5
Residual-density descriptors applied to the final multipole refinement on experimental data for $S(N^tBu)_3$ with increasing spatial resolution of the residual-density grid.

For a graphical representation of $d^f(\rho_0)$, see Fig. 9.

$n_x \times n_y \times n_z$	$d^f(0)$	$\Delta\rho_0$ (e Å^{-3})	$e_{\rm gross}$ (e)	$\Delta d^f(0)$
50^3	2.7367	0.69	8.38	
100^3	2.6472	0.73	8.38	0.0895
200^3	2.5703	0.76	8.38	0.0769
500^3	2.4913	0.78	8.38	0.0790
750^3	2.4628	0.78	8.38	0.0285
1000^3	2.4445	0.78	8.38	0.0183

6.2. Truncation of the resolution

To study further the effect of parameter adjustment, the resolution of the experimental data was truncated at different

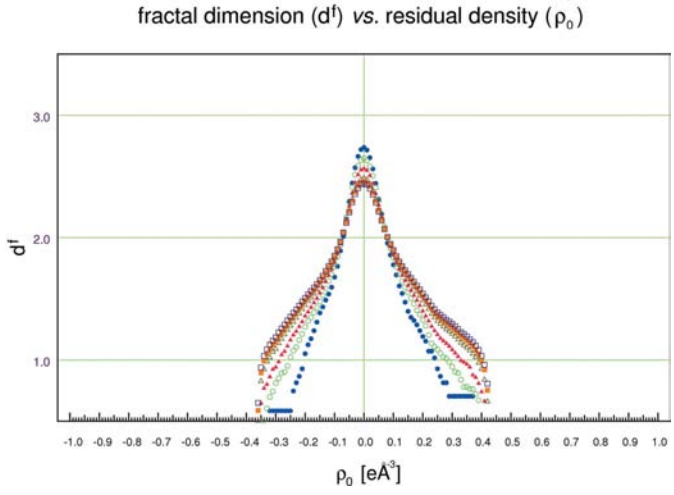

Figure 9
The grid-size dependence of the fractal dimension distribution from a converged multipole refinement on experimental data of $S(N^tBu)_3$. The colors indicate the number of grid points according to the following order: filled circles (blue), open circles (green), filled triangles (red), open triangles (olive), filled squares (orange) and open squares (violet) represent grid sizes of 50^3, 100^3, 200^3, 500^3, 750^3 and 1000^3 grid points. See also Table 5.

Table 6
Residual-density descriptors applied to experimental data for $S(N^tBu)_3$ to study truncation and refinement effects.

The experimental resolution ($\sin\theta/\lambda = 1.14$ Å^{-1}) was truncated at the indicated values. After multipole parameter refinement on the truncated data, $d^f(0)$ increases. The percentage recovered is given in the last column. $\Delta d^f = 100(d^f_{x,\mathrm{ref}} - d^f_x)/(d^f_{1.14} - d^f_x)$; x is resolution, $d^f_{x,\mathrm{ref}}$ refined at resolution x.

$(\sin\theta/\lambda)_{\max}$ (Å^{-1})	$d^f(0)$	$\Delta\rho_0$ (e Å^{-3})	e_{gross} (e)	Δd^f (%)
1.14	2.7366	0.69	8.39	
1.10	2.7256	0.66	8.01	
1.10 (refined)	2.7262	0.66	8.01	5.45
1.05	2.7121	0.61	7.58	
1.05 (refined)	2.7132	0.60	7.55	4.49
1.00	2.6989	0.53	7.25	
1.00 (refined)	2.7006	0.53	7.18	4.51
0.80	2.6543	0.35	6.27	
0.80 (refined)	2.6566	0.34	6.06	2.80

levels and the residual-density descriptors were evaluated. Then, ten cycles of a multipole refinement were carried out with the parameter values from the fully converged model as starting values and the calculated residual-density grid was again evaluated. The results are shown in Table 6. Truncation of the experimental resolution 1.14 Å^{-1} at *e.g.* 1.05 Å^{-1} leads to a reduction in $d^f(0)$ from 2.7366 to 2.7121, an increase of flatness (from 0.69 to 0.61 e Å^{-3}) and a reduced total error as indicated by e_{gross}, which falls from 8.39 to 7.58 e. After ten cycles of all parameter refinement, $d^f(0)$ reaches 2.7132 which increase is equal to 4.49% of the total loss in $d^f(0)$ due to the truncation. The parameter adjustment also improves the other quality measures. Even for a truncation at 0.80 Å^{-1}, the parameter adjustment reduces e_{gross} by 0.21 e and 2.80% of the loss in $d^f(0)$ can be recovered. Conversely, this obviously means that 97.2% of the loss in $d^f(0)$ is due to truncation only. It will be shown later (§6.3) that starting from an IAM the value $d^f(0)$ is increased after convergence of the multipole model by 0.02 (Table 7). The small increase in $d^f(0)$ summarizes the total progress made. Therefore, in IA and multipole modeling, we generally interpret a decrease in $d^f(0)$ as a decrease in the residual-density quality.

A more detailed analysis shows that in general the deviation from an ideal value of $d^f(0)$, calculated from ideal data with ideal noise equal to the experimental noise, is the appropriate measure. This ideal value is usually larger than those derived from a MM, therefore a reduction in $d^f(0)$ may serve as an indicator for residual-density quality decrease.

With this interpretation, the reduced flatness as gained by a truncation of the resolution is compensated by a reduced value of $d^f(0)$. The loss of approximately 0.08 in $d^f(0)$ due to truncation exceeds by far the gain in a multipole refinement of 0.02.

6.3. The steps of a multipole refinement

We applied the residual-density descriptors *a posteriori* to the individual steps of a multipole refinement on $S(N^tBu)_3$. The residual-density descriptors are shown in Fig. 10 and Table 7. All refinements were performed with $I > 3\sigma(I)$. For the calculation of the residual-density grid, no cut-off was applied.

Comparing the residual-density descriptors of the starting IAM with the final multipole model shows that the fractal dimension increased in total from 2.6681 (starting model) to 2.6922 (final model). We interpret this increase in $d^f(0)$ as a decrease of the features in the residual-density distribution. The features in the residual-density distribution from a spherical-atom model can at least partly be removed by a multipole model. The difference $\Delta d^f(0) = d^f_{\mathrm{final}}(0) - d^f_{\mathrm{start}}(0) = 0.0241$ quantifies this progress. The residual density becomes flatter (that is an increase in flatness) as can be seen from the decrease in $\Delta\rho_0$ from 1.29 to 0.57 e Å^{-3}. Finally, the total effect on the gross residual electrons is a reduction from 11.54 to 7.20 e. The difference gives the number of electrons, which are described by the multipole model but not by the IAM. The final 7.20 gross residual electrons contain all remaining model errors (*e.g.* from inadequatenesses of the multipole model and from data-processing errors) as well as noise in the data. We will identify later that one source of error was a tiny disorder. That the final model still ignores systematic features in the residual density can be seen from Fig. 10. The prominent shoulders of the starting model (green open circles) are to a high degree removed in the final model (olive filled diamonds), however, the final shape is not a parabola. This at once indicates the presence of a source of systematic error(s).

To the details of Table 7: after refinement of the scale factor, the coordinates of all atoms, the anisotropic displacement parameters of non-H atoms and the isotropic displacement parameters for the H atoms for an IAM, resulting from a fully converged refinement with *SHELXL* (Sheldrick & Schneider, 1997; Sheldrick, 2008), the maximum fractal dimension is $d^f(0) = 2.6681$, the number of gross residual electrons is 11.54 e and the flatness is 1.29 e Å^{-3} (green open circles). The positive residual-density distribution has a round shoulder on a high fractal dimension level where on average $F_{\mathrm{obs}} > F_{\mathrm{calc}}$, which corresponds to the bonding- and lone-pair electrons which are badly described by the independent-atom model. The large shoulder in the negative residual-density part is interpreted as the contribution from those regions in which $F_{\mathrm{obs}} < F_{\mathrm{calc}}$, *i.e.* spatial regions which have less electron density than modeled by the IAM due to bonding, and formation of a molecule, *i.e.* polarized density, charge transfer to other atoms and to the molecule as a whole.

A high-order refinement of the scale factor, coordinates and vibrational parameters of non-H atoms against $(\sin\theta/\lambda) > 0.6$ Å^{-1} yields a dramatically increased maximum fractal dimension of 2.7669 and a significantly reduced number of 4.96 gross residual electrons (blue filled circles). It is well known that much of the information about the bonding density is contained in the low-order data (Jeffrey & Cruickshank, 1953), which have been excluded from the refinement. Therefore, it is not too surprising that the quality measures indicate progress. This progress, however, is not so much owed to a progress in the model but more to fitting the data to the model by truncation of structure factors mainly describing the

Table 7
Quality measures applied *a posteriori* to each step of a multipole refinement on experimental data of $S(N^tBu)_3$.

For more information, see text. The colors and symbols in brackets refer to the residual-density distribution in Fig. 10.

	$d^f(0)$	$\Delta\rho_0$ (e Å^{-3})	e_{gross} (e)
IAM (starting model; green open circles)	2.67	1.29	11.54
$xyz + U_{ij}$ non-H ($\sin\theta/\lambda > 0.6$ Å^{-1}) (blue filled circles)	2.77	0.45	4.96
$P_v + \kappa$ non-H (red open triangles)	2.61	0.85	13.47
P_{lm} (turquoise filled triangles)	2.66	0.71	9.07
κ' non-H (pink open squares)	2.66	0.71	8.93
$xyz + U_{ij}$ non-H + RESET (violet filled squares)	2.61	0.67	12.10
$P_v + P_{lm} + \kappa$ (orange open diamonds)	2.69	0.61	7.38
$P_v + P_{lm} + \kappa + \kappa'$ (final model; olive filled diamonds)	2.69	0.57	7.20

unaccounted density due to chemical bonding. Moreover, the refined parameters have to describe only a part of the data.

In the next step (red open triangles), the monopole populations of all atoms and the expansion/contraction parameters κ for the monopoles of the non-H atoms were refined against the full experimental data [with $I > 3\sigma(I)$, as already mentioned earlier]. This leads to a decrease of residual density in the left shoulder of the distribution, whereas the right shoulder stays close to the starting distribution because the monopoles and κ account for the charge transfer and for the screening of the atomic nuclei, but not for the polarization of density. This step leads to a decrease in $d^f(0)$ to 2.61 and an increase in e_{gross} to 13.47 e, *i.e.* these two quality measures indicate a decrease in model quality, whereas $\Delta\rho_0 =$ 0.85 e Å^{-3} indicates an increase in model quality compared to the starting model. One should not forget that all other parameters are fixed at their values attained from a refinement against high-order data and that only a few parameters are allowed to adjust in each single step. The positional and vibrational parameters, which were compromised in the independent-atom model due to the assumed spherical symmetry, have been adjusted to their high-order values. The multipole parameters, which account for the deviation from the spherical symmetry, have not been adjusted yet. Therefore, it is also not surprising that the total error as given by e_{gross} increased, whereas the residual-density distribution has become flat. It is expected that the total error falls below the value from the IAM as soon as the multipoles are switched on. This should also lead to a reduction in the round shoulder of the positive residual-density distribution. That this is the case, indeed, can be seen from the next step.

The refinement of the scale factor and the monopole and multipole parameters for all atoms (turquoise filled triangles in Fig. 10) yields an increase in $d^f(0)$ from 2.6111 to 2.6592 and a decrease in $\Delta\rho_0 = 0.71$ e Å^{-3} and in the gross residual electrons from 13.47 to 9.07 e. The difference of 4.4 e was moved, *i.e.* 4.4 electrons were in total spatially appropriately re-distributed. This is a much smaller number than all bonding and lone-pair electrons in the molecule, however, a part of those electrons was already described by the spherical models. Therefore, these 4.4 e can be identified with the polarization density. As a result of the adjustment of density parameters describing aspherical features, the residual-density distribution becomes symmetric and the round shoulder in the positive residual density disappears.

The adjustment of the scale factor and κ' of the non-H atoms (pink open squares) does not lead to distinct changes in the descriptors or in the residual-density distribution.

The violet filled squares in Fig. 10 show the result from a least-squares adjustment of the scale factor, the coordinates for all atoms as well as anisotropic displacement parameters for the heavy (= non-H) atoms and an isotropic displacement for the H atoms. The distances between the sp^3-hybridized C atoms and their bonded H atoms were reset to 1.085 Å. This leads again to a higher value in e_{gross} and to a reduced value in $d^f(0)$. As for the H atoms only the isotropic displacement parameters were refined, the density parameters are not at their optimum values. This leads again to a round shoulder in the positive residual density. This positive residual density stemming from localized regions prevents the change of the sign in this region, which decreases the maximum value of the fractal dimension of the residual density.

Giving the density model parameters the opportunity to describe also the asphericities around the H atoms by adjusting the scale factor, monopole and multipole parameters for all atoms, and κ for the heavy atoms (orange open diamonds) results in the most distinct increase in $d^f(0)$ from 2.6133 to 2.6918 and to the lowest value for the gross residual electrons of 7.38 e, with the exception of the high-order refinement, in which experimental data have been excluded and which is therefore not directly comparable to the other steps of the multipole refinement. Also, the shoulder in the positive residual density disappears again.

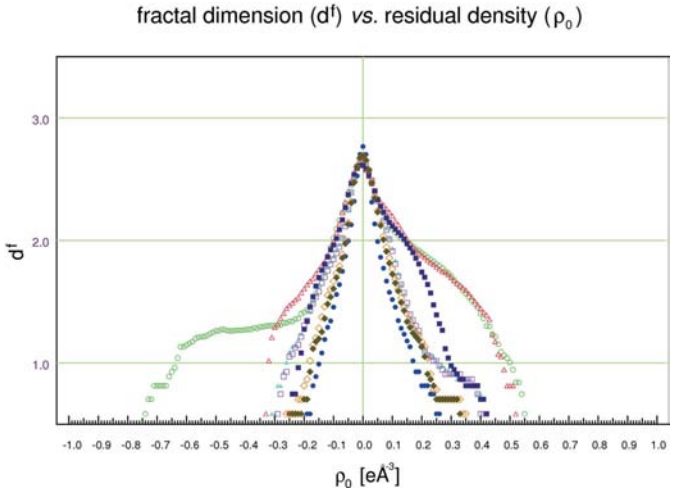

Figure 10
Progression of the fractal dimension during a multipole refinement on experimental data of $S(N^tBu)_3$. For more information and the description of the multipole refinement see text and Table 7. The experimental resolution was $(\sin\theta/\lambda)_{max} = 1.14$ Å^{-1}.

The final refinement (olive filled diamonds) of monopole and multipole population parameters for all atoms as well as κ and κ' for non-H atoms results in the highest value of $d^f(0) = 2.6922$, and the lowest values for $\Delta\rho_0 = 0.57$ e Å^{-3} and $e_{\rm gross} = 7.20$ e.

In total, the multipole model led to a decrease in the number of gross residual electrons from 11.54 (IAM) to 7.20 e (final), to a decrease in $\Delta\rho_0$ from 1.29 (IAM) to 0.57 e Å^{-3} (final) and to an increase in $d^f(0)$ from 2.6681 (IAM) to 2.6922 (final). This is interpreted as the ability of the multipole model to describe the molecular electron density in greater detail, thereby reducing the total error as given by $e_{\rm gross}$, flattening the residual density as given by $\Delta\rho_0$ and also reducing the features in the spatial distribution of the residual density as given by the increase in $d^f(0)$.

The final shape of the distribution, however, is not parabolic, due to a tiny disorder, which was too small for a refinement. To investigate this disorder, which can be generated by a 60° rotation about the central S atom in the molecular plane, we calculated the residual-density descriptors in a small volume at the supposed position of one disordered N atom. The edge length of the cube was set to 0.6 Å and a residual-density grid was calculated. The gross residual density in this volume is 0.03 e Å^{-3} and the net residual density is 0.06 e Å^{-3}. A positive value of $\rho_{\rm net}$ indicates missing (not-modeled) density. The ratio $-2 \leq \rho_{\rm net}/\rho_{\rm gross} \leq 2$ is 2 within the given accuracy. This indicates that all of the errors are due to missing density. A plot of the fractal dimension distribution of this volume is shown in Fig. 11. The numerical values of $d^f(\rho_0)$ must not be compared directly to the other plots, as the spatial resolution differs. However, there is a shift towards positive residual-density values and $d^f(0)$ is not the maximum value. For an ideal model, the maximum of the fractal dimension distribution would be at $\rho_0 = 0$ e Å^{-3} for any sufficiently large volume of the unit cell.

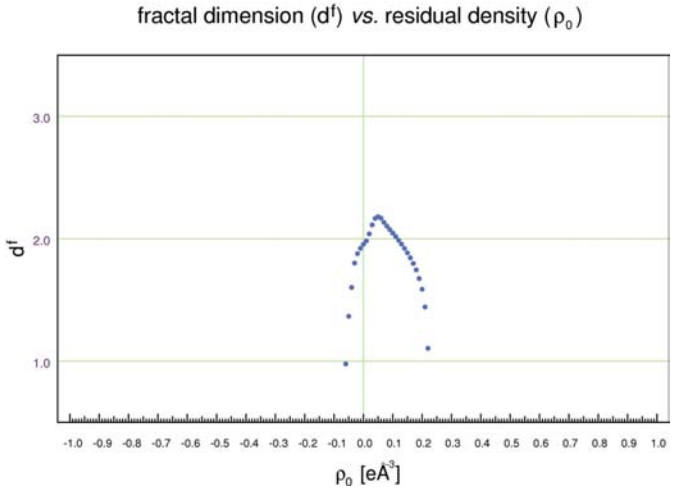

Figure 11
Fractal dimension distribution in a cube of 0.6 Å edge length around a disordered N atom in S(N^{t}Bu)$_3$. The disorder was not taken into account in the multipole model.

6.4. Extinction correction

A refinement of the extinction parameter in *SHELXL* of bullvalene trisepoxide (Liang *et al.*, 2005)[2] was performed. For testing the influence of the extinction parameter on the residual density, the options EXTI and LIST 6 were set in *SHELXL*. LIST 6 together with EXTI produces a file with file name extension 'fcf' containing $|F_{\rm meas}|^2$ which are corrected for extinction. A Perl script was developed to extract these $|F_{\rm meas}|^2$ and their corresponding standard deviations from the '*.fcf' file and to convert them to a *SHELX* format '*.hkl' file. This was imported into *XD* to produce a residual-density grid file with *XDLSM* (ten cycles of least-squares refinement) and *XDFOUR*. The same procedure was applied to $|F_{\rm meas}|^2$ which were not corrected for extinction. From the resulting distributions of $d^f(\rho_0)$ (Figs. 12 and 13) and the corresponding Table 8, it can be seen that the extinction correction changes the shape of $d^f(\rho_0)$ and the residual-density descriptors considerably: $e_{\rm gross}$ falls from 30.30 to 11.00 e, the flatness increases from 0.66 to 0.29 e Å^{-3} and the fractal dimension of zero residual density increases from 2.41 to 2.53. The shape of the distribution $d^f(\rho_0)$ is much more parabolic after extinction correction.

6.5. Separation of noise and structural information

Besides the identification and quantification of errors, another important aim of residual-density analysis is to separate noise from structural information in the residual density. This can be achieved by first evaluating $e_{\rm gross,exp}$ from the experimental data with the best model one can find. If this model describes all structural information in the data, then what is left must be noise (tacitly assuming that no data-processing errors are present).

In a second step, simulated (h, k, l, I) data are generated from this model (which is done each time a residual-density grid is calculated) and the resulting structure factors are multiplied with a Gaussian random number according to equations (19) with a guess for the noise control parameter p_1. $e_{{\rm gross},p_1}$ from noisy simulated data is compared to $e_{\rm gross,exp}$ and p_1 is steadily increased/decreased until $e_{{\rm gross},p_1} \approx e_{\rm gross,exp}$. From the plot of the fractal dimension distribution of the simulated data, one can extract the ideal values for $d^f(0)_{p_1}$ and $\Delta\rho_{0,p_1}$ and compare these to the values from the experiment. When $d^f(0)_{p_1} > d^f(0)_{\rm exp}$, there is still structural information in the residual density and the model could in principle be improved. It might turn out that the multipole model is not

[2] $C_{10}H_{10}O_3$, $M = 178.18$, orthorhombic, space group $P2_12_12_1$, $a = 6.336\,(2)$, $b = 9.250\,(2)$, $c = 13.171\,(2)$ Å, $\alpha = \beta = \gamma = 90°$, $V = 771.9\,(3)$ Å^3, $Z = 4$, $\rho_{\rm calcd} = 1.533$ Mg m^{-3}, $\mu = 0.942$ mm^{-1}, extinction coefficient 0.049 35 (240). 14 311 reflections were measured ($\theta_{\rm max} = 58.95°$, 1100 independent reflections, $R_{\rm int} = 0.0303$). Final $R_1 = 0.0226$ for 119 refined parameters and 1100 reflections with $I \geq 2\sigma(I)$, wR_2(all data) = 0.0578, GOF = 1.106, absolute structure parameter 0.01 (19). X-ray data were collected on a Bruker SMART CCD 6000 diffractometer at 100 (2) K with mirror-monochromated Cu $K\alpha$ radiation. The structure was solved by direct methods using *SHELXS-97* (Sheldrick, 1990) and refined against $|F|^2$ on all data by full-matrix least squares with *SHELXL-97* (Sheldrick & Schneider, 1997). Non-H atoms were refined with anisotropic displacement parameters, H atoms were placed in calculated positions and refined using a 'riding model'.

flexible enough to allow for these improvements for example due to a limited flexibility of the radial functions or due to the frozen cores. However, in this case, the radial functions or core densities could be improved. When $d^f(0)_{p_1} < d^f(0)_{\rm exp}$, the experimental data were over-fitted and a part of the noise was absorbed into the density model. This is of particular importance in MEM. For a practical application, compare the blue and green symbols in Fig. 14. In this case, it is obvious from the large shoulders in the periphery that the model is not perfect. If it is nevertheless assumed that all experimentally determined 8.38 gross residual electrons are from noise only, the shape would appear as depicted by the green filled triangles. Although the numerical difference in $d^f(0)$ is small [$d^f(0)_{p_1=0.222} = 2.68$, $d^f(0)_{\rm exp} = 2.65$], it is seen that model improvements are possible, especially if this value is compared

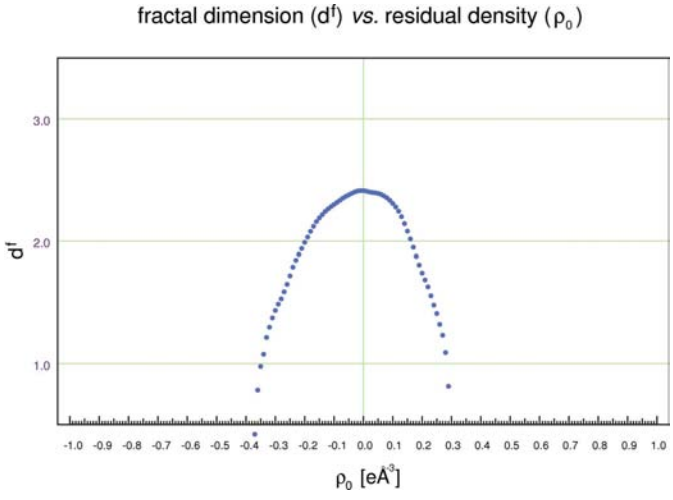

Figure 12
The fractal dimension distribution of the residual density of bullvalene trisepoxide (IAM). No extinction correction was applied. For more information, see Table 8.

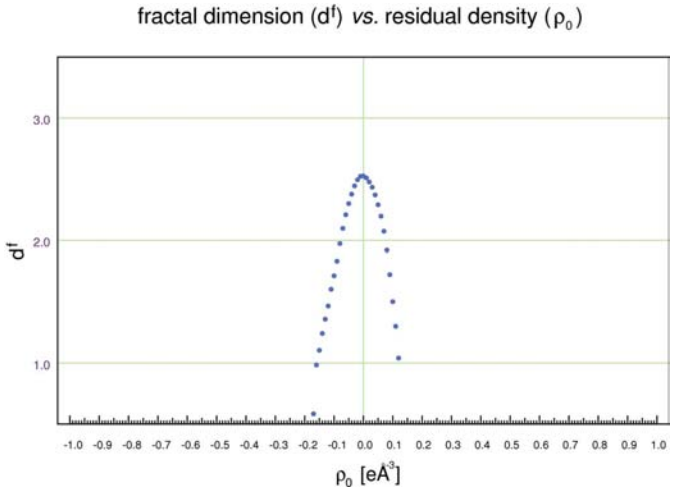

Figure 13
The fractal dimension distribution of the residual density of bullvalene trisepoxide (IAM). An extinction correction was applied in *SHELXL*. For more information, see Table 8.

Table 8
Residual-density descriptors applied to experimental data for bullvalene trisepoxide to study the effects of extinction correction as implemented in *SHELXL*.

The experimental resolution was $\sin\theta/\lambda = 0.56$ Å^{-1}. For the distribution $d^f(\rho_0)$, see Figs. 12, 13.

	$d^f(0)$	$\Delta\rho_0$ (e Å^{-3})	$e_{\rm gross}$ (e)
Correction off	2.41	0.66	30.30
Correction on	2.53	0.29	11.00

to the total increase of $d^f(0)$ due to the application of MM from §6.3, which was 0.02, accompanied by a reduction in $e_{\rm gross}$ of approximately 4 e. So, small differences in $d^f(0)$ may correspond to large differences in $\Delta\rho_0$ and $e_{\rm gross}$ (see Table 7). Of course, real improvements in the density model would lead to a reduced value for $e_{\rm gross,exp}$ (and reduced $\Delta\rho_0$) and a new noise control parameter $p_{1,\rm new} < p_{1,\rm old}$ had to be determined. This is an iterative procedure, which in the end yields a final noise-control parameter and identical residual distributions from simulated and experimental data.

7. Summary and future applications

The fractal dimension distribution of the residual density brings all residual-density distributions to one and the same scale: the maximum value of $d^f(\rho_0)$ indicates the experimental resolution together with the grid spacing, the width indicates the flatness. The minimum and maximum values of the residual density appear as limiting values in the fractal dimension distribution. These indicate the flatness of the residual-density distribution. The shape indicates the presence/absence of systematic errors. Noise can be separated from structural information still contained in the residual density by comparison of simulated and experimentally determined

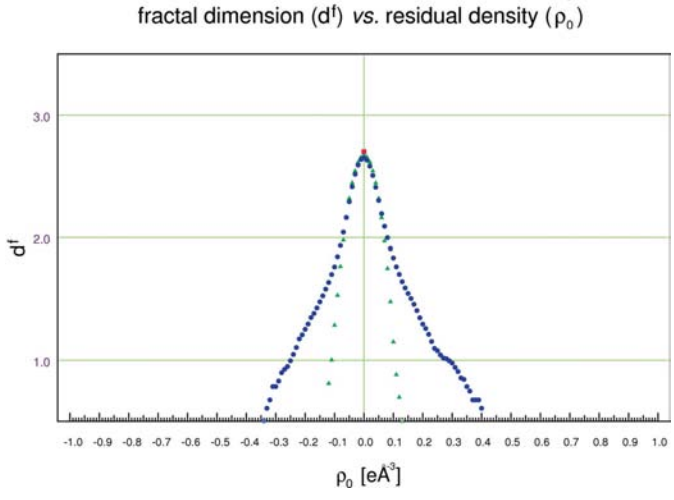

Figure 14
Noise added to simulated data for S(N^{t}Bu)$_3$. Red filled square: noise control parameter $p_1 = 0.000$. Green filled triangles: $p_1 = 0.222$, yielding the same $e_{\rm gross} \approx 8.4$ e as in the experiment. Blue filled circles: experiment.

distributions of the residual density with an identical total error as given by the number of the gross residual electrons. These indicate noise and model errors. The simulated residual-density distribution is obtained from the best density model one can find plus noise, which is added to the intensities. Comparing these distributions also reveals features in the residual density. These are quantified by the difference in $d^f(\rho_0)$. Therefore, this value can be used as a limiting value or as a target figure. Any progress in modeling can be identified and quantified by the developed measures, whether the progress be in density modeling, *e.g.* development of more flexible radial functions, or improved core densities, change to other pseudo-atom descriptions like invarioms or Hirshfeld atoms, or in data processing, *e.g.* by application of corrections to the experimental data. The method allows the comparison of residual densities obtained from different methods such as multipole models, invariom models, wavefunction and density-matrix fitting, and maximum-entropy methods. The measures are applicable in a local and in a global way by appropriately choosing the volume to be analyzed. Although applied in this paper mainly to high-resolution cases, the measures are very general and can also be employed in protein crystallography or other fields and they are easily extended to higher dimensions and to the evaluation of momentum densities.

Potential future applications:

(i) will help to make a decision in the case of two models having similar figures of merit, but possibly different density distributions; this situation appears *e.g.* in refinements of non-centrosymmetric space groups;

(ii) as a diagnostic tool for neglected symmetry in standard structure determination;

(iii) convergence check, stopping criterion in MM and MEM;

(iv) improvement of refinement strategies;

(v) improvement of radial functions;

(vi) improvement of atom scattering factors;

(vii) investigation of systematic errors due to inadequate or missing oblique incidence corrections for detectors.

The developed concepts are being currently implemented into the *XD* and *WinGX* (Farrugia, 1999) program packages.

APPENDIX *A*

The maximum contribution to the difference density from a phase error of π:

$$\begin{aligned}\Delta\mathbf{F} &= \mathbf{F}_{\rm obs} - \mathbf{F}_{\rm calc}\\ &= F_{\rm obs}\exp(i\phi_{\rm obs}) - F_{\rm calc}\exp(i\phi_{\rm calc})\\ &= \{F_{\rm obs}\exp[i(\phi_{\rm obs}-\phi_{\rm calc})] - F_{\rm calc}\}\exp(i\phi_{\rm calc})\\ &= [F_{\rm obs}\exp(i\pi) - F_{\rm calc}]\exp(i\phi_{\rm calc})\\ &= -(F_{\rm obs}+F_{\rm calc})\exp(i\phi_{\rm calc})\\ \rightarrow |\Delta\mathbf{F}| &= (F_{\rm obs}+F_{\rm calc}).\end{aligned}$$

Although the deviation of the maximum error due to a phase error may appear over-simplified, a more detailed analysis yields the same result (see *e.g.* Coppens, 1997).

We acknowledge scientific support by and encouraging discussions in particular with Professor Farrugia, Professor Koritsanszky, Professor Sheldrick, Professor van Smaalen, and Professor Stalke and the members of his work group. Special thanks go to Dr Leusser and Professor Stalke for providing the experimental data on $S(N^tBu)_3$. Burkhard Heisen gave valuable hints for software development. One of the authors (JH) is grateful to the DFG priority programme SPP 1178 'Experimental charge density as the key to understand chemical interactions' for financial support.

References

Brewer, J. & Di Girolamo, L. (2006). *Atmos. Res.* **82**, 433–454.
Bronstein, I. N., Semendjajew, K. A., Musiol, G. & Mühlig, H. (1993). *Taschenbuch der Mathematik*. Frankfurt am Main: Verlag Harry Deutsch.
Bruker (2006). *XPREP – Programm zur Bearbeitung von Beugungsdaten und Untersuchung reziproker Gitter*. Bruker AXS Inc., Madison, WI, USA.
Collins, D. M. (1982). *Nature (London)*, **298**, 49–51.
Coppens, P. (1997). In *X-Ray Charge Densities and Chemical Bonding*, *IUCr Texts on Crystallography*, No. 4. Oxford University Press/IUCr.
Farrugia, L. J. (1999). *J. Appl. Cryst.* **32**, 837–838.
French, S. & Wilson, K. (1978). *Acta Cryst.* A**34**, 517–525.
Gilmore, C. J. (1996). *Acta Cryst.* A**52**, 561–589.
Hansen, N. K. & Coppens, P. (1978). *Acta Cryst.* A**34**, 909–921.
Jeffrey, G. A. & Cruickshank, D. W. J. (1953). *Q. Rev. Chem. Soc.* **7**, 335–376.
Leusser, D., Henn, J., Kocher, N., Engels, B. & Stalke, D. (2004). *J. Am. Chem. Soc.* **126**, 1781–1793.
Liang, S., Lee, C.-H., Kozhushkov, S. I., Yufit, D. S., Howard, J. A. K., Meindl, K., Rühl, S., Yamamoto, C., Okamoto, Y., Schreiner, P. R., Rinderspacher, B. C. & de Meijere, A. (2005). *Chem. Eur. J.* **11**, 2012–2018.
Palatinus, L. & van Smaalen, S. (2005). *Acta Cryst.* A**61**, 363–372.
Rollet, J. S. (1988). *Crystallographic Computing 4; Techniques and New Technologies*, edited by N. W. Isaacs & M. R. Taylor, pp. 149–166. Oxford: Oxford Science Publications.
Sakata, M. & Sato, M. (1990). *Acta Cryst.* A**46**, 263–270.
Sheldrick, G. M. (1990). *Acta Cryst.* A**46**, 467–473.
Sheldrick, G. M. (2008). *Acta Cryst.* A**64**, 112–122.
Sheldrick, G. M. & Schneider, T. R. (1997). *Methods Enzymol.* **277**, 319–343.
Volkov, A., Macchi, P., Farrugia, L. J., Gatti, C., Mallinson, P., Richter, T. & Koritsanszky, T. (2006). *XD2006 – A Computer Program Package for Multipole Refinement, Topological Analysis of Charge Densities and Evaluation of Intermolecular Interaction Energies from Experimental and Theoretical Structure Factors*. University at Buffalo, State University of New York, NY, USA; University of Milano, Italy; University of Glasgow, UK; CNRISTM, Milano, Italy; Middle Tennessee State University, TN, USA.